19. Mineralogy and Sedimentology of Pleistocene Sediment in the South China Sea (ODP Site 1144)[1]

S. Boulay,[2] C. Colin,[2] A. Trentesaux,[3] F. Pluquet,[2, 3] J. Bertaux,[4] D. Blamart,[5] C. Buehring,[6] and P. Wang[7]

ABSTRACT

Grain size, detrital mineral, clay mineralogy (<2 µm), and major element analyses were carried out on the carbonate-free fraction of sediments from Ocean Drilling Program Site 1144 from the northern margin of the South China Sea (SCS), close to the mouth of the Pearl River. This site provides a 517-m sedimentary record extending back to 1.1 Ma. Clay content and the chemical index of alteration do not exhibit significant variation between glacial and interglacial changes, suggesting no important change in the proportion of primary to secondary minerals in the sediment. Two grain size populations were identified, 2.5–5 µm (clay) and 20–40 µm (silt). Glacial stages are characterized by higher proportions of silt size and quartz content than interglacial stages. Two hypotheses can explain these variations: (1) drier conditions associated with an intensification of winter monsoon transport of eolian loess to the northern part of the SCS during glacial periods and/ or (2) an effect of sea level changes on the detrital material transport from continent or shelf to the deep ocean.

INTRODUCTION

One of the major components of the tropical climate system is the Asian monsoons, which result in a differential land-sea sensitive heating, inducing seasonal reversals in wind direction and producing intensive rainfall during the summer. Numerous paleoclimatic studies

[2]FRE 2566 ORSAYTERRE, Université Paris-Sud, 91405 Orsay Cedex, France. Correspondence author: colin@geol.u-psud.fr
[3] FRE 2255 CNRS, Sédimentologie et Géodynamique, Université des Sciences et Technologies de Lille-SN5, F-59655 Villeneuve d'Ascq Cedex, France.
[4]UR Paléotropique, Centre IRD, 72 route d'Aulnay, 93143 Bondy Cedex, France.
[5]Laboratoire des Sciences du Climat et de l'Environnement, Laboratoire mixte CNRS-CEA, Avenue de la Terrasse, 91198 Gif-sur-Yvette Cedex, France.
[6]Institut fur Geowissenschaften Geologie, 24118 Kiel, Germany.
[7]Laboratory of Marine Geology, MOE, Tongji University, 1239 Siping Road, Shanghai, 200092, People's Republic of China.

(Clemens and Prell, 1991; Wang et al., 1999), based on different proxies, have led to the reconstruction of the strength of the paleomonsoon intensity. Such reconstructions have shown that variations in summer monsoon intensity are mainly forced by the contrast in insolation between the Northern and Southern Hemispheres (Clemens et al., 1991). When the summer insolation in the Northern Hemisphere decreases relative to present-day conditions, the low-pressure surface cell over the Asian continent is weaker. This results in a reduced land-sea pressure gradient and a weak summer monsoon, whereas increased summer insolation strengthens the summer monsoon (Clemens and Prell, 1990; Emeis et al., 1995).

On a regional scale, the climate of the South China Sea (SCS) and the ambient land masses is dominated by the East Asian monsoon, which represents an important factor driving weathering and erosion of the eastern Asian region. On geological timescales, changes in the strength of the summer monsoon rainfall and the winter monsoon wind have led to a modification of the chemical and physical weathering intensity of the East Asian continent (e.g., the Pearl River Basin) and of the eolian dust transportation patterns. Therefore, SCS sediments as well as the loess plateau provide records of the variability of the intensity in the erosion of the Asian continent, which is in turn related to paleoclimatic and paleoenvironmental variations affecting southeast Asia. Past East Asian monsoon variations have been extensively studied from Chinese loess plateau deposits using several proxies, such as grain size, magnetic susceptibility, or mineral distribution (An et al., 1990; Xiao et al., 1995; Chen et al., 1997; Lu et al., 2000; Porter and An, 1995). Similar studies of deep-sea sediments of the SCS, however, have seldom been performed (Wang et al., 1999).

The main purpose of this pilot study is to reconstruct from deep-sea sediment the paleoenvironmental changes affecting the continent by (1) characterizing the mineralogy, the grain size distribution, and the geochemistry of major elements in the Pleistocene sediments from the northern part of the SCS over the last 1.1 Ma, (2) identifying the sources of these sediments, and (3) establishing the relationship between the variability of siliciclastic sediments and the climatic changes including monsoon and sea level changes during the Quaternary.

MATERIALS AND METHODS

Materials

Ocean Drilling Program (ODP) Site 1144 was drilled on the northern margin of the SCS (20°3.18′N, 117°25.14′E) in ~2037 m water depth, with a maximum penetration of 452 meters below seafloor (mbsf). This site is at the same location as core 17940 (*Sonne-95* cruise) (Fig. F1) and is considered particularly suitable for high-resolution paleoenvironmental reconstitutions of the last glacial period (pollen, siliciclastic grain size, etc.) (Sarnthein et al., 1994; Wang et al., 1999). Site 1144, located ~400 km off the Hong Kong shore and the Pearl River mouth, was drilled on a seamount in order to avoid turbidites. The lithology throughout the recovered section is quite homogeneous and is dominated by terrigenous silty clay with quartz silt and nannofossil carbonate ooze. Other minor lithologies including low proportions of sponge spicules and diatoms were also observed (Fig. F2B). Carbonate contents

F1. Topographic map of the SCS, p. 13.
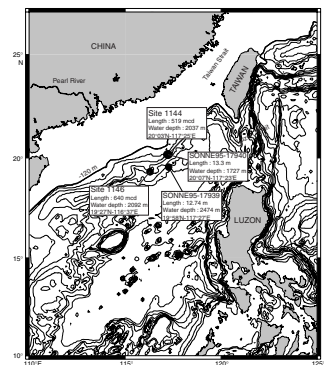
F2. Sediment accumulation rate, p. 14.
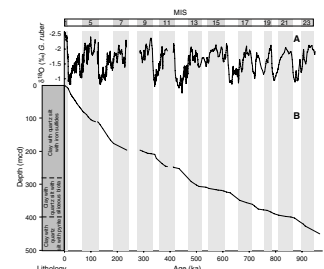
are quite low and range from 10 to 20 wt% (Shipboard Scientific Party, 2000).

The stratigraphy of Site 1144 was established using (1) biostratigraphic datums (Shipboard Scientific Party, 2000; Shyu et al., this volume), (2) nine radiocarbon ^{14}C datings (five datings on mixed bulk planktonic foraminifers [Chen et al., this volume] and four datings based on samples of the planktonic foraminifers *Globigerina ruber* and *Globigerina sacculifer* [Buehring et al., this volume]), and (3) the high-resolution δ^{18}O record from the planktonic foraminifer *G. ruber*, using two references: the δ^{18}O stack of Bassinot et al. (1994) for the upper 413 meters composite depth (mcd), and below (413–517 mcd), the ODP Site 677 δ^{18}O record, as age reference. Site 1144 provides a sedimentary record extending back to marine isotopic Stage (MIS) 23 (Fig. F2A). This site presents small hiatuses during MIS 5.5 and MIS 11 as well as a 50-k.y. hiatus that comprises the lower part of MIS 7.5 and most of MIS 8.

The age (ka) vs. depth (mcd) diagram (Fig. F2B) shows a downcore decrease in sedimentation rates and higher sedimentation rates during glacial stages than interglacial stages. Such changes could be explained by (1) changes in the terrigenous supply to the SCS, (2) changes in the biogenic productivity, and/or (3) changes in the lithology that would provide differential compaction. The compaction has an important effect on the long-term downcore sedimentation rate decrease. However, as no important changes in lithology were observed between glacial and interglacial changes, it is unlikely that differential compaction has a major effect on the sediment between adjacent glacial and interglacial stages. Therefore, compaction cannot explain the important variations in sedimentation rates observed during glacial and interglacial stage changes. At Site 1144, glacial stages are characterized by an increase in sedimentation rates in agreement with the sedimentation rates calculated for several piston cores of the northern part of the SCS (Huang and Wang, 1998). This increase in sedimentation rates could be attributed to an increase in terrigenous supply, as the biogenic material (silica and carbonate) does not vary significantly between glacial and interglacial changes.

Site 1144 is characterized by high sedimentation rates (average = ~48 cm/k.y.) that are particularly suitable for high-resolution paleoenvironmental reconstitution. Hole 1144A was sampled at 150-cm intervals for grain size and mineralogical and geochemical investigations.

Methods

Grain-size distribution measurements of carbonate-free sediment were carried out on a Malvern Mastersizer X apparatus following the procedure described in detail by Trentesaux et al. (2001). A 100-μm lens was used, allowing an analytical grain size range of 1–160 μm. Bulk sediments were first suspended in deionized water and gently shaken to achieve disaggregation. Ultrasound was used before pouring the sediment into the laser grain sizer in order to decrease the degassing time of the water. The suspension was then gently poured into the fluid module of the granulometer. After a first run, hydrochloric acid in excess was injected to obtain the carbonate-free fraction grain size distribution. Sonication was not used to complete the sediment dispersion, as previous measurements have shown that the use of ultrasonic dispersion has a dramatic effect on some particles such as foraminifers or vesicular volcanic glass. Grain size distributions of the carbonate-free fraction still include a small portion of marine opal.

Clay mineralogy determinations were performed at the University of Orsay by standard X-ray diffraction (XRD) on the carbonate-free, <2-μm size fraction, following the procedure described by Holtzapfell (1985). The <2-μm clay fraction was isolated by gravitational settling. X-ray diffractograms were made on a Kristalloflex (Siemens) X-ray diffractometer from 3.5° to 30°2θ using CuK$_\alpha$ radiation. Three tests were performed on the oriented mounts: (1) untreated, (2) glycolated (12 hr in ethylene glycol), and (3) heated at 500°C for 2 hr. Diffractograms showed the presence of different minerals including quartz and feldspars. Clay minerals are composed of illite, chlorite, kaolinite, smectite, and complex mixed-layer minerals. These mixed-layer clays were mainly assigned to randomly mixed illite-smectite species, and they will be referred to as "smectites" in the text. The semiquantitative composition of the clay fraction was obtained by measuring the peak areas of basal reflections on XRD diagrams using the MacDiff software (Petschick, 1997).

Quartz and carbonate contents of the bulk fraction were determined by Fourier transform infrared (FTIR) spectroscopy (Pichard and Fröhlich, 1986). The samples were ground in acetone to a particle size of <2 μm with small agate balls in an agate vial and kept at 4°C to prevent heating and structural changes. The powder was then mixed with KBr in an agate mortar with a dilution factor of 0.25%. A 300-mg pellet, 13 mm in diameter, was pressed into a vacuum die with up to 8 t/cm² of compression. For each sample, an infrared spectrum averaging 50 scans in the 4000- to 250-cm^{-1} energy range with a 2-cm^{-1} resolution was recorded using a Perkin-Elmer FT 16 PC spectrometer.

Major element content analyses were performed using an electron microprobe on glass samples obtained after fusion of the sediment (Colin et al., 1998). The carbonate fraction was removed by leaching 50 mg of sediment with 20% acetic acid in an ultrasonic bath, followed by rinsing several times and centrifuging to remove traces of carbonate solution. The carbonate-free fraction was subsequently carefully mixed by hand with 20% Li$_2$CO$_3$ SPMerck in an agate mortar. The mixture was fused in air on a platinum cell by radio frequency induction heating. The cell was heated to 900°C during 15 s to drive H$_2$O and CO$_2$ from the sample, and the temperature was then increased sufficiently above the mixture liquidus to ensure complete melting of the sample. Minimum temperatures required for rapid and complete fusion were established by trial and error and range from 1300° to 1450°C for the studied sediments. Similar techniques have been previously applied by Nicholls (1974) and Brown (1977) for major element content analysis.

Taking into account the sedimentation rates and the sampling intervals (one sample every 150 cm), grain size analyses were performed with a chronological resolution of 1–4 k.y. for the last 300 k.y. and 4–10 k.y. for the older period. Clay mineralogy determinations and major element content analyses were performed with the same chronological resolution only for the last 400 and 250 k.y., respectively.

RESULTS

Siliciclastic Grain Size

Values of mean grain size plotted vs. time in Figure F3A show limited variations between 6 and 28 μm, which are mostly silt size. However, a detailed examination of this curve indicates that interglacial stages are characterized, on average, by slightly finer grains (~10–15 μm for MIS 1,
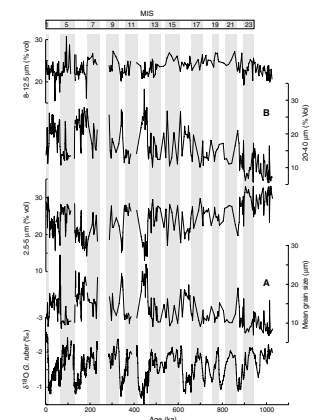
5, 7, 9, 11, 13, 15, 19, 21, and 23) than glacial periods (~16–26 µm for MIS 2, 3, 4, 6, 10, 12, 16, 20, and 22). Besides, a long-term increase in grain-size can be observed prior to 600 ka. Such glacial–interglacial variations are confirmed on Figure F4, which shows different grain size distributions for interglacial (Holocene; 5.7 mcd) and glacial (Stage 6; 166.7 mcd) samples.

Previous studies on grain size variations (e.g., Wang et al., 1999) have used the standard grain size classification (clay = <6 µm and silt = 6 to >63 µm) to represent grain size variations through time. Here, we propose a new method, permitting easy identification of the grain size intervals with the highest variability along a sedimentary sequence. For each 30 grain size classes given by the Malvern Mastersizer, standard deviations were calculated for our 300 samples. Standard deviation values vs. grain size classes are displayed on Figure F5. Two peaks are observed in this plot, at 2.5- to 5- and 20- to 40-µm grain size intervals, respectively. Each of these size classes represents a population of grains with the highest variability through time. On the other hand, for instance, the intermediate 8- to 12.5-µm size class is characterized by low standard deviation values, implying no important change of the proportion of this grain size population in the siliciclastic fraction. This result is confirmed by the variations of the 2.5- to 5-, 8- to 12.5-, and 20- to 40-µm size class proportion (percent) through time (Figs. F4, F3B). Both the 2.5- to 5- and 20- to 40-µm grain size populations vary significantly with climate changes. No significant variation can be observed in the 8- to 12.5-µm grain size population (Fig. F3B). Long-term fluctuations of the 2.5- to 5-µm size class distribution are inversely correlated to those of the 20- to 40-µm size class. Interglacial stages are characterized by higher proportions of the 2.5- to 5-µm size interval than glacial stages.

Clay and Bulk Mineralogy

Throughout the entire Site 1144 sediment sequence, illite and chlorite are the dominant clay minerals and are in the range of 30%–60% and 15%–35% of the <2-µm clay mineral fraction, respectively (Fig. F6A). Smectite and kaolinite are of secondary importance, reaching values of 0%–30% and 5%–25%, respectively. These ranges are close to those observed for Site 1146 (Trentesaux et al., this volume).

Over the last 400 k.y. no major change in clay mineral composition was recorded. There is a slight increase in chlorite during glacial Stages 2, 3, 6, and 10. There appears also to be a slight increase (decrease) in smectite (illite) during isotopic events 1, 3, 5.1, and 7.1, resulting in an increase of the smectite/(illite+chlorite) ratio.

Quartz and carbonate contents of the bulk fraction were determined by FTIR spectroscopy on 29 samples to compare the proportion of quartz with grain size and major element results. Quartz proportions were corrected for carbonate dilution using the following relationship:
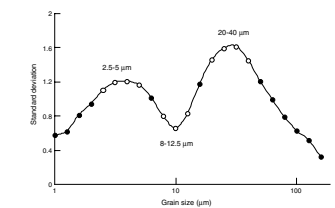
$$\% \; Qz_{cor.} = \% \; Qz_{mes.} \; /(100 - \% \; CaCO_3) \times 100.$$

Quartz proportions vary significantly with climate changes (Fig. F6B). Observed values are lower during MIS 1, 4, and 5 than during MIS 2, 3, and 6.
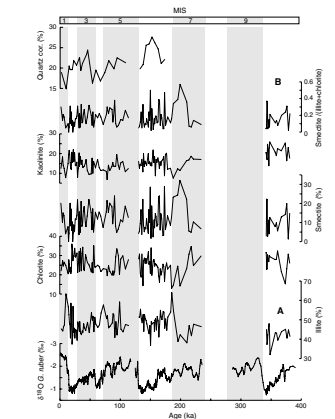
F4. Grain size classes in interglacial and glacial samples, p. 16.
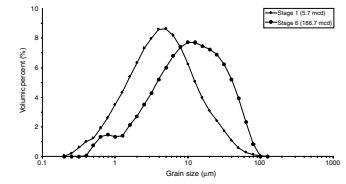
F5. Standard deviation vs. grain size class, p. 17.

F6. Clay minerals, smectite/(illite+chlorite), and quartz, p. 18.

Major Elements

Major element content analyses were performed on 87 samples (Fig. F7). CaO, Na_2O, TiO_2, and FeO do not present any significant variation during glacial–interglacial changes and range between 0.3 and 1.7, 1 and 1.6, 1 and 1.3, and 4 and 7.3 wt%, respectively. On the contrary, SiO_2, Al_2O_3, K_2O, and MgO contents vary significantly with climatic changes from 64 to 73, 15 to 20, 2.9 to 4.3, and 1.6 to 2.8 wt%, respectively. Al_2O_3, K_2O, and MgO display the same behavior, with an increase during interglacial Stages 1 and 5 and a decrease during glacial Stages 2, 3, 4, and 6. MIS 6.5 is also characterized by an increase of these elements. SiO_2 percent variations are opposite from those of Al_2O_3 and K_2O. Normalization to aluminum is commonly used to characterize terrigenous sediments. SiO_2/Al_2O_3 and K_2O/Al_2O_3 as well as SiO_2/K_2O ratios are displayed on Figure F8. Interglacial Stages 1 and 5 are characterized by lower values of the SiO_2/Al_2O_3 and SiO_2/K_2O ratios than during glacial Stages 2, 3, 4, and 6. The K_2O/Al_2O_3 ratio does not exhibit any significant variation along the entire record.

DISCUSSION

Sediment Sources

Major element contents of the sediment (Fig. F7) at Site 1144 are very similar to those of a granite. This suggests that the detrital material of the northern part of the SCS could be derived from a siliceous igneous source with no major contribution of basic igneous rocks, such as the basaltic volcanoes of the Luzon arc (Fig. F1).
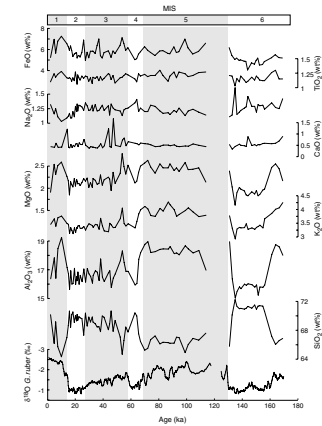
The Pearl River is the second largest river supplying the SCS in water discharge (320 km³/yr) with a modern sediment discharge of ~95 × 10⁶ t/yr. Its catchment area (~442,600 km²) is mainly composed of Precambrian and Phanerozoic granitic rocks at the outcrop. The Pearl River thus appears to be the main contributor of detrital material to the northern part of the SCS. However, detrital material inputs from Taiwan ranges and/or from the East China Sea through the Taiwan Strait (Fig. F1) may also have contributed to Site 1144 sediments. Eolian sediment is an another potential source of detrital material to the SCS (Wang et al., 1999) and will be discussed below.
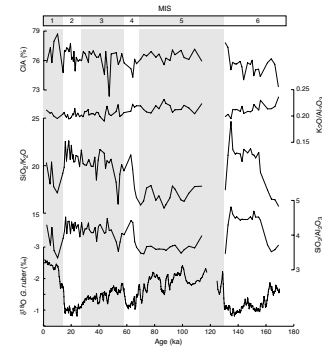
Clay and Bulk Mineralogy Changes

Numerous paleoclimatic studies have shown that clay mineral contents change through time as a result of climate modifications (Bouquillon et al., 1990; Fagel et al., 1994; Colin et al., 1999, 2001). To understand the meaning of changes in clay mineral composition, it is necessary to document the origins and potential source areas of minerals in the SCS sediment. Two groups of minerals can be distinguished:

1. Quartz, illite, and chlorite: quartz is a primary mineral and is abundant in igneous and metamorphic formations. Both illite and chlorite may derive either from the degradation of muscovite and biotite from metamorphic and igneous formations or from the erosion of sedimentary rocks (Chamley, 1989). Chlorite is also a common "primary" mineral of low-grade metamorphic rocks. Consequently, illite, chlorite, and quartz can be consid-

ered as mainly primary minerals, deriving from physical erosion or moderate chemical weathering.

2. Smectite and kaolinite: both smectite and kaolinite are formed by the hydrolysis of primary minerals in the Pearl River plain soils where detrital material is deposited and altered. The source of kaolinite and smectite is located in the downstream parts of the catchment of the Pearl River where lateritic red earths (ferralitic soils) and red earths (bisialitic soils) are dominant (Ségalen, 1995). Such soils are mainly composed of secondary minerals.

Consequently, the smectite/(illite+chlorite) ratio can be used as a proxy for the intensity of chemical weathering and/or physical erosion on the continent. For Site 1144, the smectite/(illite+chlorite) ratio values exhibit a restricted range from 0 to 0.6 with no clear relation to glacial–interglacial changes except for a slight increase during the warm isotopic Substages 1, 5.1, 6.3, 6.5, and the end of MIS 7.

In order to assess the degree of chemical weathering of terrigenous detritus experienced prior to marine deposition, the chemical index of alteration (CIA)

$$CIA = \text{molar ratio } [Al_2O_3/(Al_2O_3+Na_2O+K_2O+CaO_{inorganic}) \times 100],$$

introduced by Nesbitt and Young (1982), was also calculated from major element results (Fig. F8). This last parameter quantifies more precisely the effect of chemical weathering on the rocks by loss of the labile elements Na, Ca, and K. CIA for all feldspars = 50%, and the mafic minerals biotite, hornblende, and pyroxenes have CIA values = 50%–55%, 10%–30%, and 0%–10%, respectively. The secondary clay minerals and chlorite CIA values = 100%, and illite and smectite CIA values = 70%–85%. Consequently, the CIA reflects the proportions of primary and secondary minerals in bulk samples. It has been used as a climatic indicator in the Andaman Sea sediment where it is well correlated with the mineralogical record (Colin et al., 1998). CIA values obtained from Site 1144 exhibit a restricted range between 73% and 79% (Fig. F8), typical of altered rocks, suggesting low variations of the proportion of primary and secondary minerals in bulk sediment. This is in agreement with the small changes observed in the smectite/(illite+chlorite) ratio. A slight increase in the CIA values can be observed only in the earliest Holocene, during the warm MIS 5.1 and 5.3, and during the MIS 6–MIS 5 transition. At Site 1144, the sediment does not seem to have recorded any important changes in the intensity of the chemical weathering affecting the continent.

From the quartz concentration records through the last 180 k.y., displayed on Figure F9, it appears that minima coincide with interglacial periods, whereas during isotopic Stages 2, 3, and 6, quartz values are higher. There is no clear correlation between quartz and specific clay mineral composition (Fig. F6). However, long-term fluctuations of quartz are well correlated to SiO_2 variations (Fig. F9). An increase in quartz is characterized by an increase in SiO_2, suggesting that variations of SiO_2 mainly depend on quartz input. The SiO_2/Al_2O_3 ratio can also be controlled by hydrolysis during chemical weathering. As CIA values and clay distribution exhibit minor changes, we suggest that this ratio mainly reflects changes in the proportion of silt quartz and clay mineral content proportions. An increase in the SiO_2/Al_2O_3 ratio is attributed to an increase of the quartz proportion and a decrease of the aluminosili-

F9. $\delta^{18}O$, L*, $CaCO_3$, quartz, grain size, and SiO_2/Al_2O_3, p. 21.
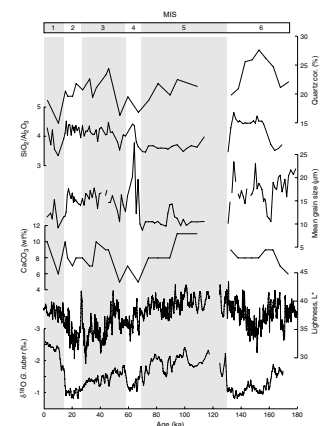
cate fraction. As K_2O is mainly linked to the aluminosilicate fraction, variations of the SiO_2/K_2O ratio could also signify the same pattern.

Significance of Siliciclastic Grain Size Variations

Site 1144 grain size variations are similar to those obtained from cores 17940 and 17939 (Fig. F1) collected during the *Sonne-95* cruise in the same area (Wang et al., 1999). In core 17940, the clay (<6 µm fraction) and silt (>6 µm fraction) contents present the same variations as those at Site 1144 for the last 40 k.y. The Holocene period is characterized by higher proportions of clay (70%–75%) than during the last glacial maximum (LGM) (50%–55%). Based on a simple empirical relationship (Koopmann, 1981) between the percentage of siliciclastic fine fraction (<6 µm) and the primary modal grain size of siliciclastic silt (>6 µm), Wang et al. (1999) distinguish two different sources for the clay and silt fractions. Clay and silt fractions have been mainly attributed to fluvial sediment supply and eolian input, respectively. The intensity of wet summer and dry winter monsoons thus was reconstructed from the history of continental aridity in South China, which in turn controls the fluvial and/or eolian sediment supply to the continental margin of the Pearl River mouth. On a global scale, an increase in summer monsoon rainfall implies an increase in clay supply by the Pearl River, whereas drier conditions associated with an intensification of winter monsoon transport carry more eolian loess to the northern part of the SCS.

During the last 180 k.y., grain size changes are correlated to quartz and SiO_2/Al_2O_3 variations (Fig. F9), suggesting that the silt fraction (20- to 40-µm grain size class) is mainly dependent on quartz input. Quartz is a common mineral in loess deposits of Central China (Porter and An, 1995) and has been widely studied on land or in marine sediments as an indicator of continental aridity and winter monsoon strength (e.g., Rea and Leinen, 1988; Xiao et al., 1995; Wang et al., 1999). Glacial stages are characterized by an enhanced winter monsoon that drives eastward eolian particles from the Central China deserts to the Pacific Ocean (Pettke et al., 2000; Jones et al., 1994). These may have an eolian origin at Site 1144, already supposed by Wang et al. (1999). Glacial stages are associated with a decrease in the summer monsoon rainfall and/or an increase in the winter monsoon transport. The long-term grain size increase observed between 1000 and 600 ka would be associated with global cooling, inducing drier conditions and/or an increase in the winter monsoon transport.

However, this increased supply of quartz and silt size class appears also to be correlated with a time of lowered sea level, which implies that sea level changes could also have an effect on detrital material transport from the continent or from the shelf to the deep ocean. The northern SCS shelf is wide at the Pearl River mouth and is mainly composed of sandy sediments (Wang et al., 1992). The distance from the shore to the –120-m bathymetry corresponds to ~250 km (Fig. F1), and a large part of the continental shelf emerged during the glacial low sea levels (–120 m for the LGM) (Wang et al., 1995). During high sea level stands, sediment could have been impounded on the shelf and coarser clastic deposition cut off from the margin. In contrast, during low sea level stands, the shelf was exposed to erosion and remobilized sediments were then redeposited in the deep sea. This is in agreement with higher sedimentation rates during glacial periods (Fig. F2) as well as with a

lower reflectance (L*, lightness) than that during interglacial stages (Fig. F9). This last parameter often increases with increasing carbonate calcium content (Fig. F9) and, therefore, could be a proxy of either the $CaCO_3$ productivity by both benthic and planktonic organisms or the detrital input. Consequently, glacial times are expected to show an increase of terrigenous supply to the SCS. In addition, during low sea level stands, the Pearl River mouth is located closer to Site 1144 than during high sea level, suggesting intensified bypass of suspended matter from shelf/slope into the basin. This would transport higher proportions of silt to the continental margin in front of the Pearl River mouth.

SUMMARY AND CONCLUSIONS

Detailed analysis of siliciclastic grain size in association with major element geochemistry and clay mineralogy were carried out on the carbonate-free fractions of sediments from Site 1144 on the northern margin of the SCS.

The smectite/(illite+chlorite) ratio and CIA exhibit minor changes with global climate changes, indicating that Site 1144 records no major changes of chemical weathering in the sediment source areas.

Two grain size populations with the highest variability through time were identified at 2.5–5 µm (clay) and 20–40 µm (silt). Glacial periods are characterized by higher proportions of silt size than interglacial stages. An increase in the grain size (silt proportion) can be observed between 1000 and 600 ka.

Glacial stages are also characterized by higher contents of quartz, higher sediment accumulation rates, lower reflectance (L*, lightness), and higher SiO_2/Al_2O_3 and SiO_2/K_2O ratios than interglacial periods. Glacial grain size increases seem to be mainly related to an increase in quartz content in the siliciclastic fraction.

Two hypotheses can explain such changes in sediment supply, grain size, and composition:

1. Drier conditions and intensified winter monsoon transport of eolian loess to the northern part of the SCS during glacial periods (in this case, glacial periods would be associated with a decrease in the summer monsoon rainfall and/or an increase in the winter monsoon transport), and/or
2. An effect of sea level changes in the detrital material transport from continent or shelf to the deep ocean.

ACKNOWLEDGMENTS

process XRD and major element analyses. This manuscript is dedicated to the memory of Dr. J. Bertaux, who died on 26 August 2002.

REFERENCES

An, Z., Liu, T., Lu, Y., Porter, S.C., Kukla, G., Wu, X., and Hua, Y., 1990. The long-term paleomonsoon variation recorded by the loess-paleosol sequence in central China. *Quat. Int.,* 8:91–95.

Bassinot, F.C., Labeyrie, L.D., Vincent, E., Quidelleur, X., Shackleton, N.J., and Lancelot, Y., 1994. The astronomical theory of climate and the age of the Brunhes–Matuyama magnetic reversal. *Earth Planet. Sci. Lett.,* 126:91–108.

Bouquillon, A., France-Lanord, C., Michard, A., and Tiercelin, J.-J., 1990. Sedimentology and isotopic chemistry of the Bengal Fan sediments: the denudation of the Himalaya. *In* Cochran, J.R., Stow, D.A.V., et al., *Proc. ODP, Sci. Results,* 116: College Station, TX (Ocean Drilling Program), 43–58.

Brown, R.W., 1977. A sample fusion technique for whole rock analysis with the electron microprobe. *Geochim. Cosmochim. Acta,* 41:433–438.

Chamley, H., 1989. *Clay Sedimentology:* Berlin (Springer-Verlag).

Chen, F.H., Bloemendal, J., Wang, J.M., Li, J.J., and Oldfield, F., 1997. High-resolution multi-proxy climate records from Chinese loess: evidence for rapid climatic changes over the last 75 kyr. *Palaeogeogr., Palaeoclimatol., Palaeoecol.,* 130:323–335.

Clemens, S.C., and Prell, W.L., 1990. Late Pleistocene variability of Arabian Sea summer monsoon winds and continental aridity: eolian records from the lithogenic component of deep-sea sediments. *Paleoceanography,* 5:109–145.

————, 1991. One million year record of summer monsoon winds and continental aridity from the Owen Ridge (Site 722), northwest Arabian Sea. *In* Prell, W.L., Niitsuma, N., et al., *Proc. ODP, Sci. Results,* 117: College Station, TX (Ocean Drilling Program), 365–388.

Clemens, S.C., Prell, W.L., Murray, D., Shimmield, G., and Weedon, G., 1991. Forcing mechanisms of the Indian Ocean monsoon. *Nature,* 353:720–725.

Colin, C., Bertaux, J., Turpin, L., and Kissel, C., 2001. Dynamics of the erosion in the Irrawaddy River basin during the last two climatic cycles (280–0 ka). *C. R. Acad. Sci. Paris,* 332:483–489.

Colin, C., Kissel, C., Blamart, D., and Turpin, L., 1998. Magnetic properties of sediments in the Bay of Bengal and the Andaman Sea: impact of rapid North Atlantic Ocean climatic events on the strength of the Indian monsoon. *Earth Planet. Sci. Lett.,* 160:623–635.

Colin, C., Turpin, L., Bertaux, J., Desprairies, A., and Kissel, C., 1999. Erosional history of the Himalayan and Burman ranges during the last two glacial–interglacial cycles. *Earth Planet. Sci. Lett.,* 171:647–660.

Emeis, K.-C., Anderson, D.M., Doose, H., Kroon, D., and Schulz-Bull, D., 1995. Sea-surface temperatures and the history of monsoon upwelling in the northwest Arabian Sea during the last 500,000 years. *Quat. Res.,* 43:355–361.

Fagel, N., Debrabant, P., and André, L., 1994. Clay supplies in the Central Indian Basin since the late Miocene: climatic or tectonic control? *Mar. Geol.,* 122:151–172.

Holtzapffel, T., 1985. Les minéraux argileux: préparation, analyse diffractométrique et détermination. *Publ. Soc. Geol. Nord.,* 12.

Huang, W., and Wang, P., 1998. A quantitative approach to deep-water sedimentation in the South China Sea: changes since the last glaciation. *Sci. China,* Ser. D41:195–201.

Jones, C.E., Halliday, A.N., Rea, D.K., and Owen, R.M., 1994. Neodymium isotopic variations in North Pacific modern silicate sediment and the insignificance of detrital REE contributions to seawater. *Earth Planet. Sci. Lett.,* 127:55–66.

Koopmann, B., 1981. Sedimentation von Saharastaub im subtropischen Atlantik während der letzten 25,000 Jahr. *"Meteor" Forschungsergeb. Reihe C,* 35:23–59

Lu, H., van Huissteden, K., Zhou, J., Vandenberghe, J., Liu, X., and An, Z., 2000. Variability of East Asian winter monsoon in Quaternary climatic extremes in North China. *Quat. Res.,* 54:321–327.

Nesbitt, H.W., and Young, G.M., 1982. Early Proterozoic climates and plate motions inferred from major element chemistry of lutites. *Nature,* 299:715–717.

Nicholls, I.A., 1974. A direct fusion method of preparing silicate rock glasses for energy-dispersive electron microprobe analysis. *Chem. Geol.,* 14:151–157.

Petschick, R., 1997. MacDiff 3.2.6 Manual. http://servermac.geologi.uni-frankfurt.de/Rainer.html. Johann Wolfgang Goethe-Univ. Frankfurt am Main, Germany.

Pettke, T., Halliday, A.N., Hall, C.M., and Rea, D.K., 2000. Dust production and deposition in Asia and the North Pacific Ocean over the past 12 Myr. *Earth Planet. Sci. Lett.,* 178:397–413.

Pichard, C., and Frölich, F., 1986. Note technique, analyse IR quantitatives des sédiments, exemple du dosage du quartz et de la calcite. *Rev. l'Inst. Français Pétrol.,* 1:809–819.

Porter, S.C., and An, Z., 1995. Correlation between climate events in the North Atlantic and China during the last glaciation. *Nature,* 375:305–308.

Rea, D.K., and Leinen, M., 1988. Asian aridity and the zonal westerlies: late Pleistocene and Holocene record of eolian deposition in the Northwest Pacific Ocean. *Palaeogeogr., Palaeoclimatol., Palaeoecol.,* 66:1–8.

Sarnthein, M., Pflaumann, U., Wang, P.X., and Wong, H.K. (Eds.), 1994. Preliminary Report on *Sonne-95* Cruise "Monitor Monsoon" to the South China Sea. *Rep. Geol.-Palaontol. Inst. Univ. Kiel.,* 68.

Ségalen, P., 1995. Les sols ferrallitiques et leur répartition géographique, tome 3. *éditions de l'Orstom, coll. "Etudes et thèses":* Paris, 201.

Shipboard Scientific Party, 2000. Site 1144. *In* Wang, P., Prell, W.L., Blum, P., et al., *Proc. ODP, Init. Repts.,* 184, 1–103 [CD-ROM]. Available from: Ocean Drilling Program, Texas A&M University, College Station TX 77845-9547, USA.

Trentesaux, A., Recourt, P., Bout-Roumazeilles, V., and Tribovillard, N., 2001. Carbonate grain-size distribution in hemipelagic sediments from a laser particle sizer. *J. Sediment. Res.,* 71:858–862.

Wang, L., Sarnthein, M., Erlenkeuser, H., Grimalt, J., Grootes, P., Heilig, S., Ivanova, E., Kienast, M., Pelejero, C., and Pflaumann, U., 1999. East Asian monsoon climate during the late Pleistocene: high-resolution sediment records from the South China Sea. *Mar. Geol.,* 156:245–284.

Wang, P., Wang, L., Bain, Y., and Jian, Z., 1995. Late Quaternary paleoceanography of the South China Sea: surface circulation and carbonate cycles. *Mar. Geol.,* 127:145–165.

Wang, P., Zhimin, J., and Zhiwei, L., 1992. Late Quaternary sedimentation rate in the South China Sea. *In* Ye, Z., and Wang, P. (Eds.), *Contributions to Late Quaternary Paleoceanography of the South China Sea:* Qingdao (Qingdao Ocean Univ. Press), 23–41.

Xiao, J., Porter, S.C., An, Z., Kumai, H., and Yoshikawa, S., 1995. Grain size of quartz as an indicator of winter monsoon strength on the loess plateau of central China during the last 130,000 yr. *Quat. Res.,* 43:22–29.

Figure F1. Topographic map of the South China Sea (SCS) and adjacent landmass showing locations of ODP Sites 1144 and 1146 and presite cores 17939 and 17940 from the *Sonne-95* cruise (Sarnthein et al., 1994). Present 120-m isobath shows the approximate position of the coastline during low sea level.
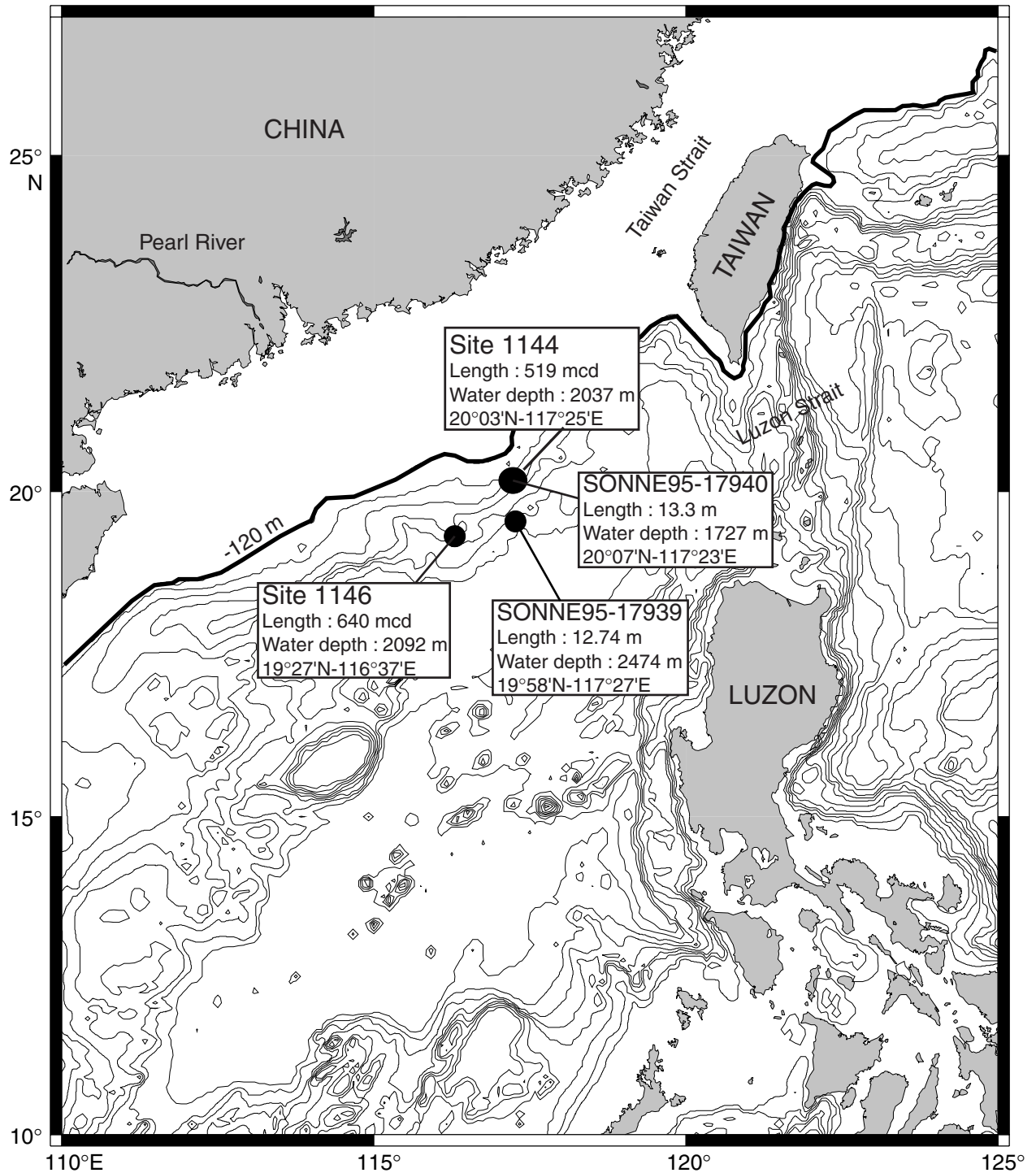
Figure F2. Variations of sediment accumulation rate for Site 1144 are linked to the planktonic foraminifer *G. ruber* δ^{18}O record. **A.** *G. ruber* δ^{18}O record. **B.** Age vs. depth diagram. MIS = marine isotopic stage.
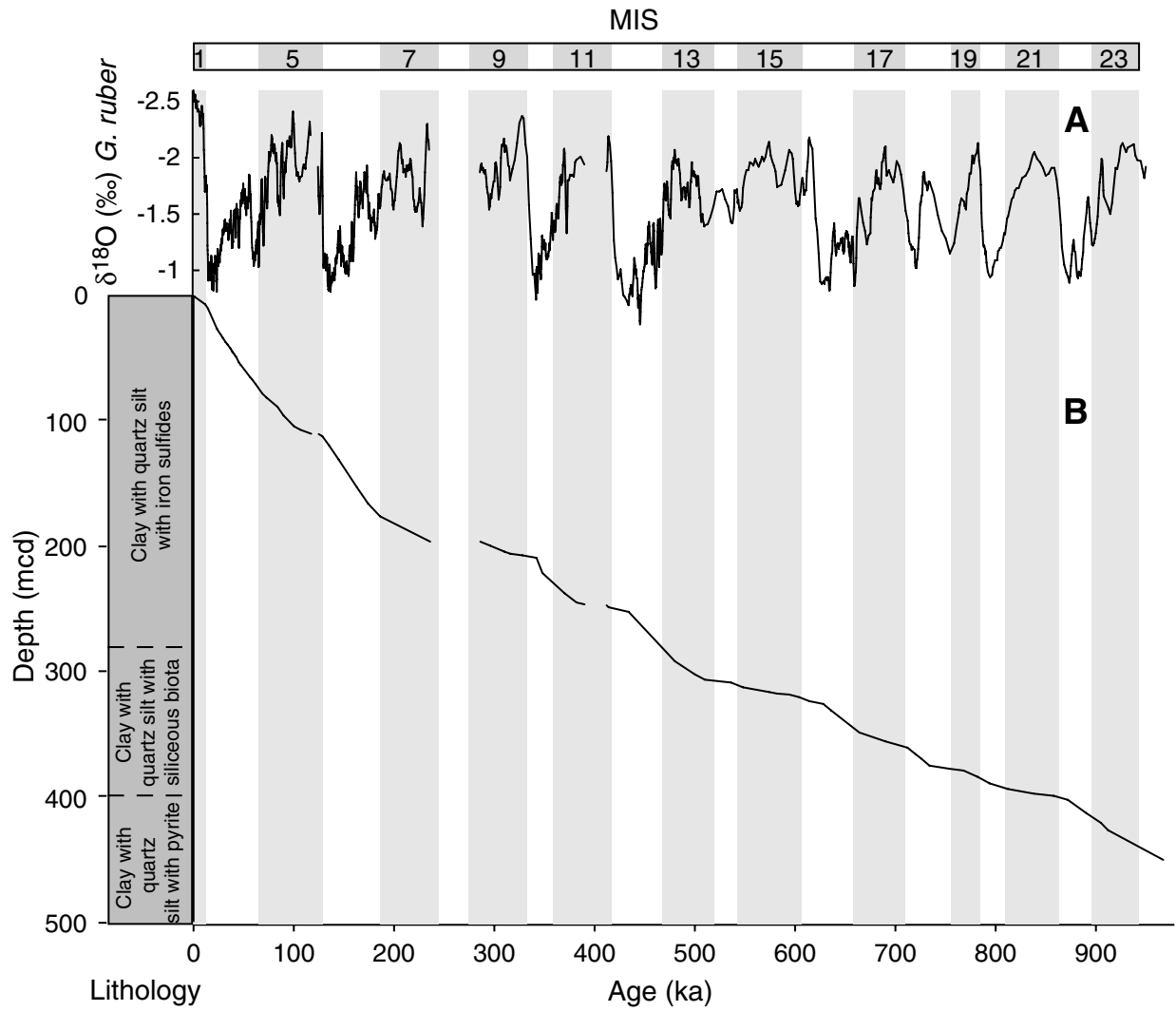
Figure F3. Planktonic foraminifer *G. ruber* δ^{18}O record vs. age. **A.** Mean grain size variations of the siliciclastic fraction vs. age. **B.** Variations of the proportion of the grain size classes 2.5–5, 8–2.5, and 20–40 µm vs. age. Shaded areas highlight interglacial stages. MIS = marine isotopic stage.
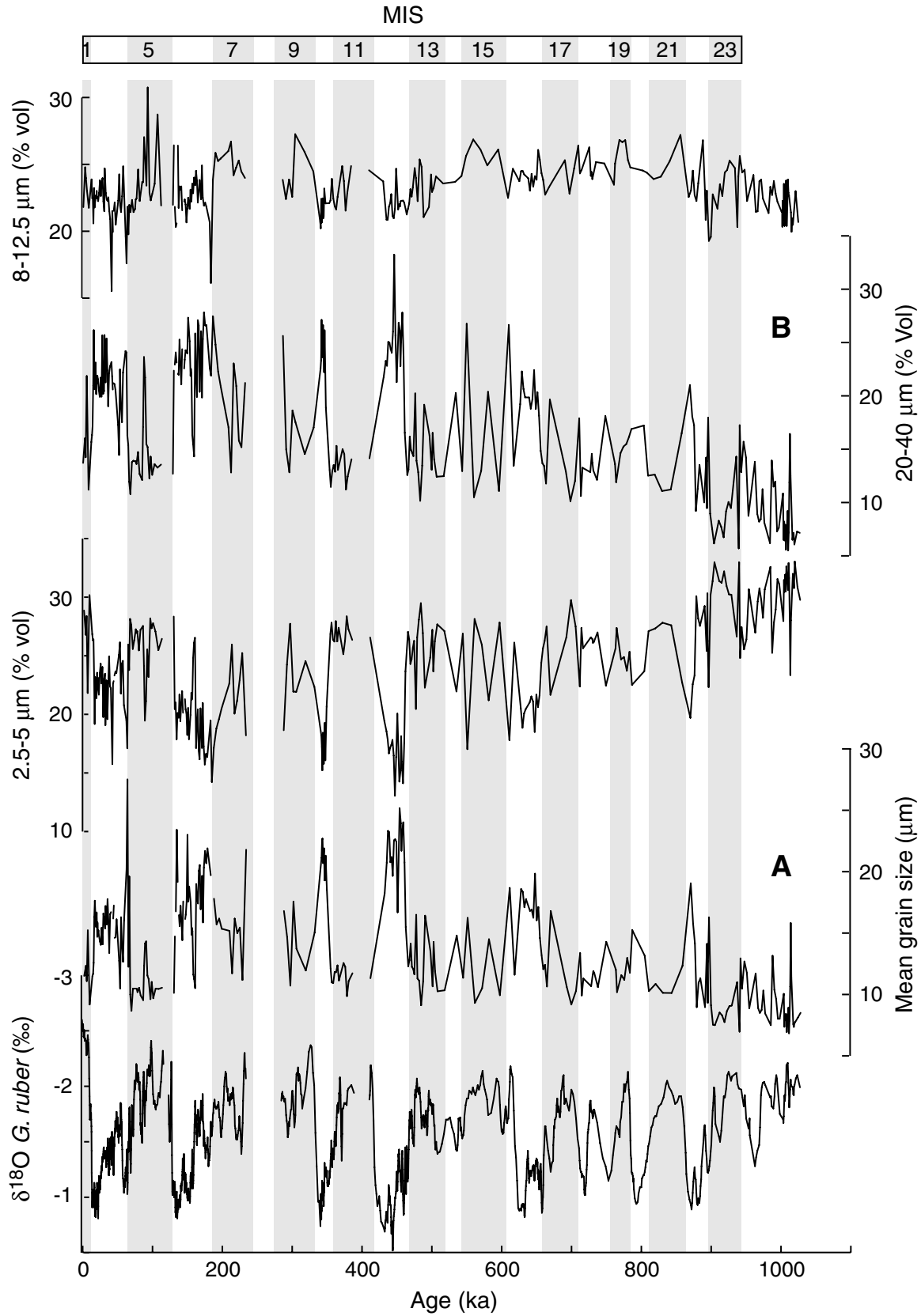
Figure F4. Volumic percent of each grain size class of interglacial and glacial samples.
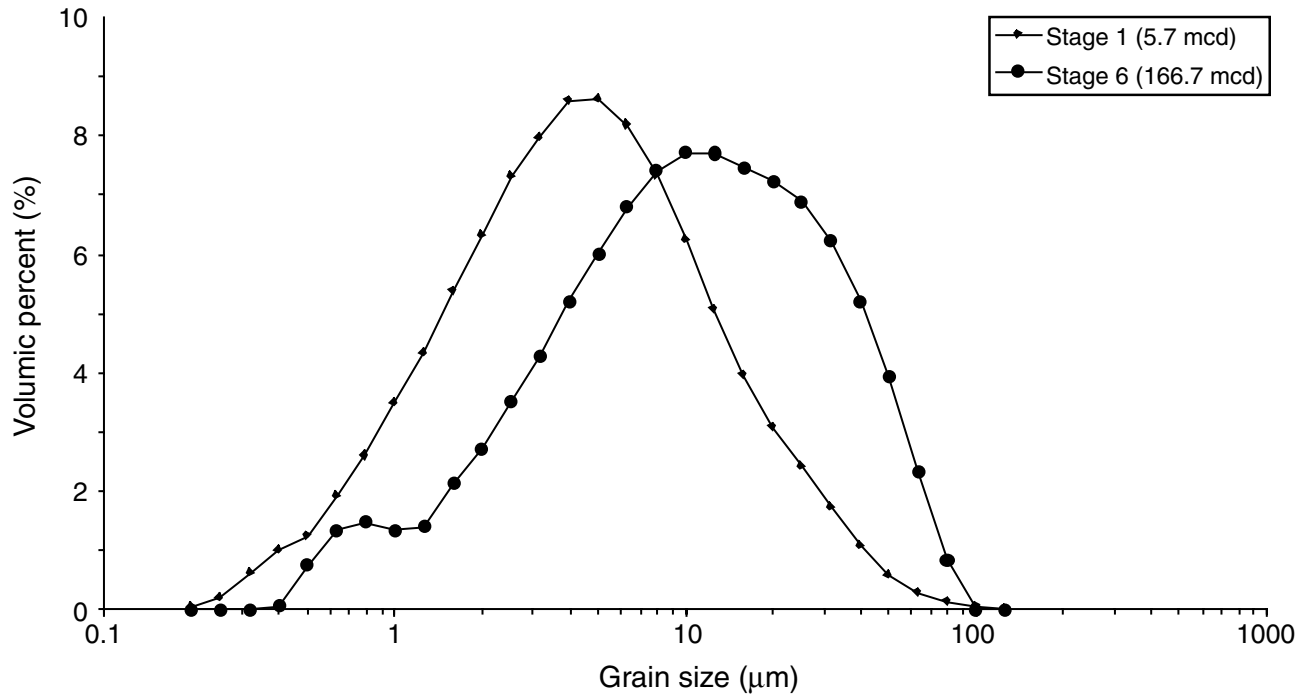
Figure F5. Standard deviation values vs. grain size class diagram. Open circles = classes taking into account the limited three populations: 2.5–5, 8–12.5, and 20–40 μm.
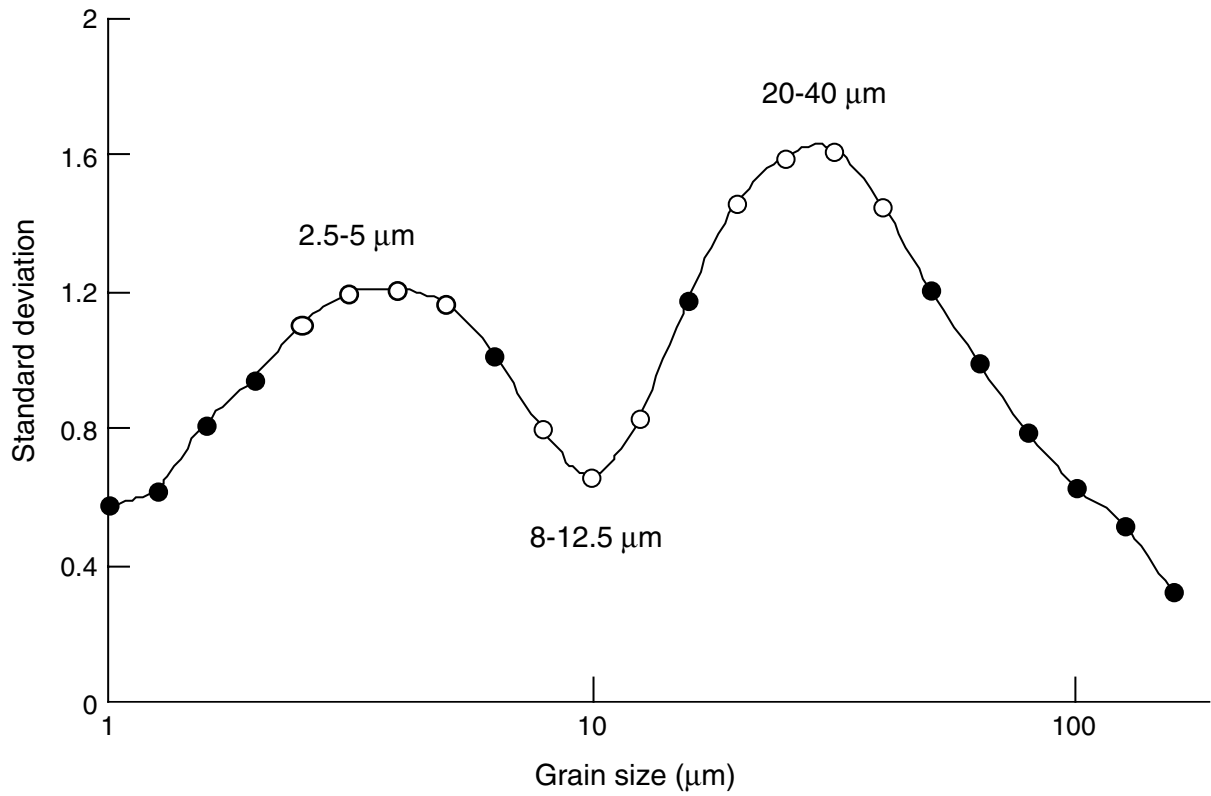
Figure F6. Planktonic foraminifer *G. ruber* $\delta^{18}O$ record vs. age. **A.** Clay mineral proportions in the <2-µm size fraction and smectite/(illite+chlorite) ratio vs. age. **B.** Quartz (corrected from carbonate dilution) content vs. age. MIS = marine isotopic stage.
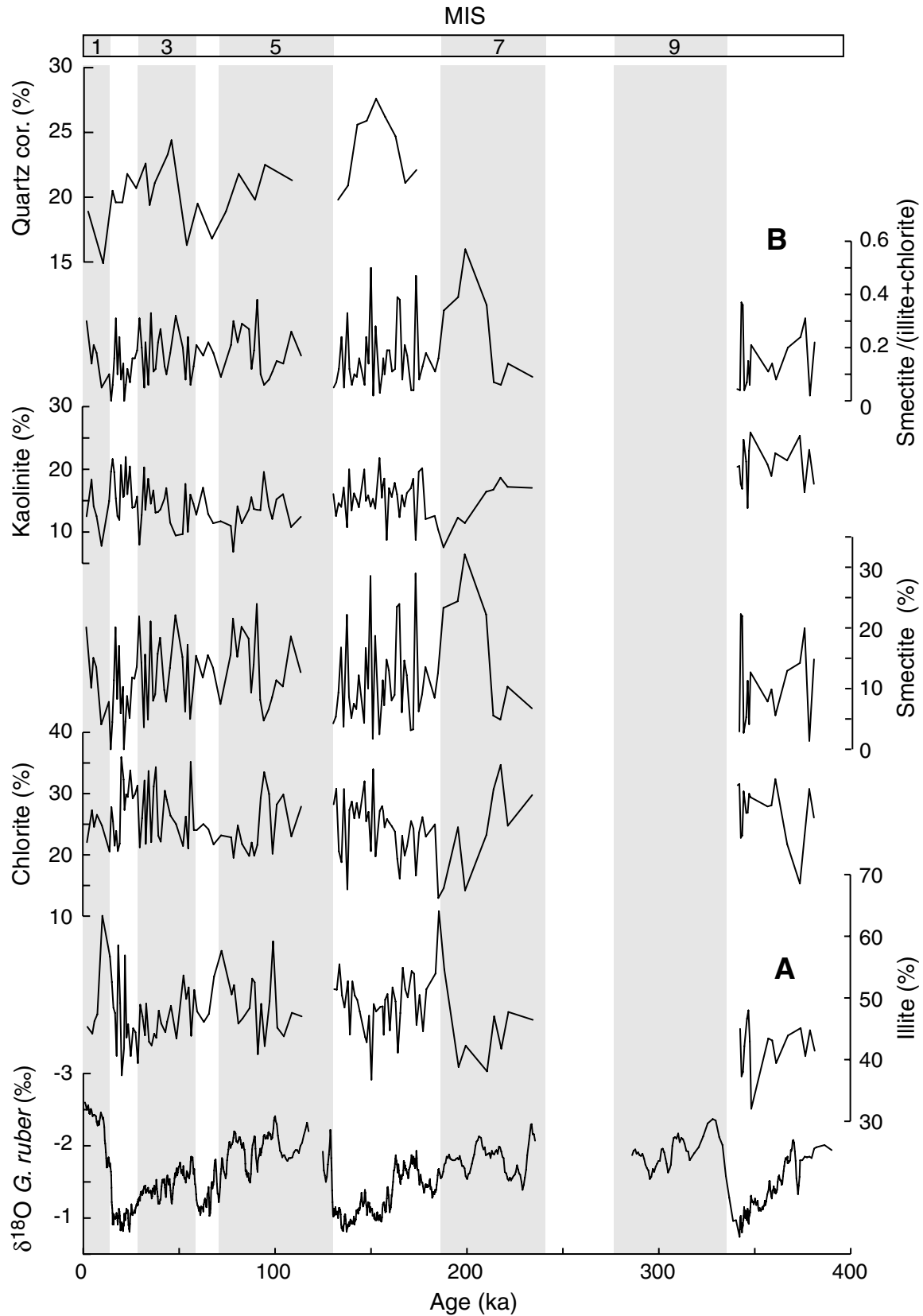
Figure F7. Planktonic foraminifer *G. ruber* $\delta^{18}O$ record and major element contents for Site 1144 vs. age. MIS = marine isotopic stage.
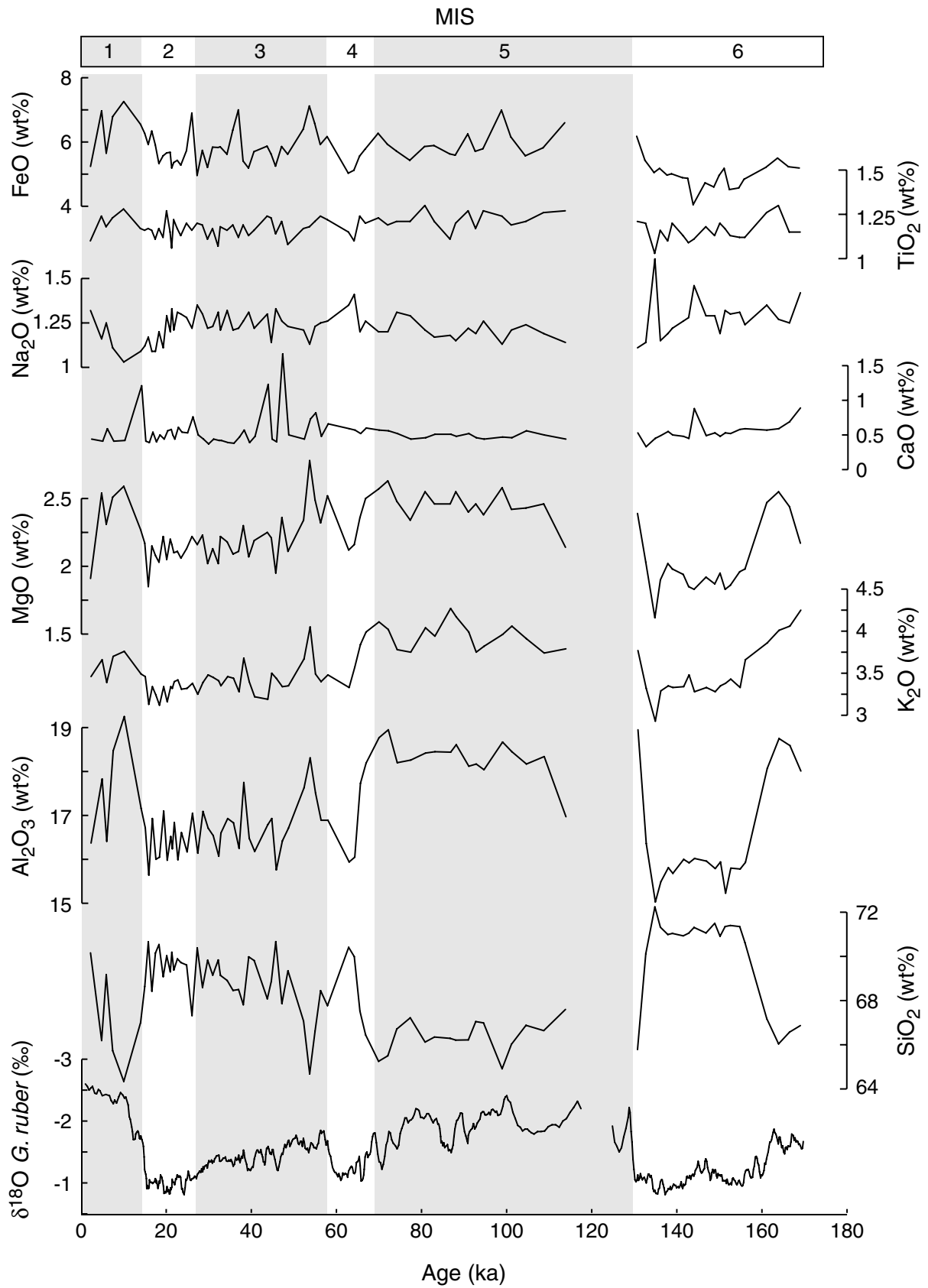
Figure F8. Planktonic foraminifer *G. ruber* $\delta^{18}O$ record, SiO_2/Al_2O_3, SiO_2/K_2O, K_2O/Al_2O_3 ratios, and CIA (CIA = molar ratio of $[Al_2O_3/(Al_2O_3+Na_2O+K_2O+CaO_{inorganic}] \times 100$) vs. age. MIS = marine isotopic stage.

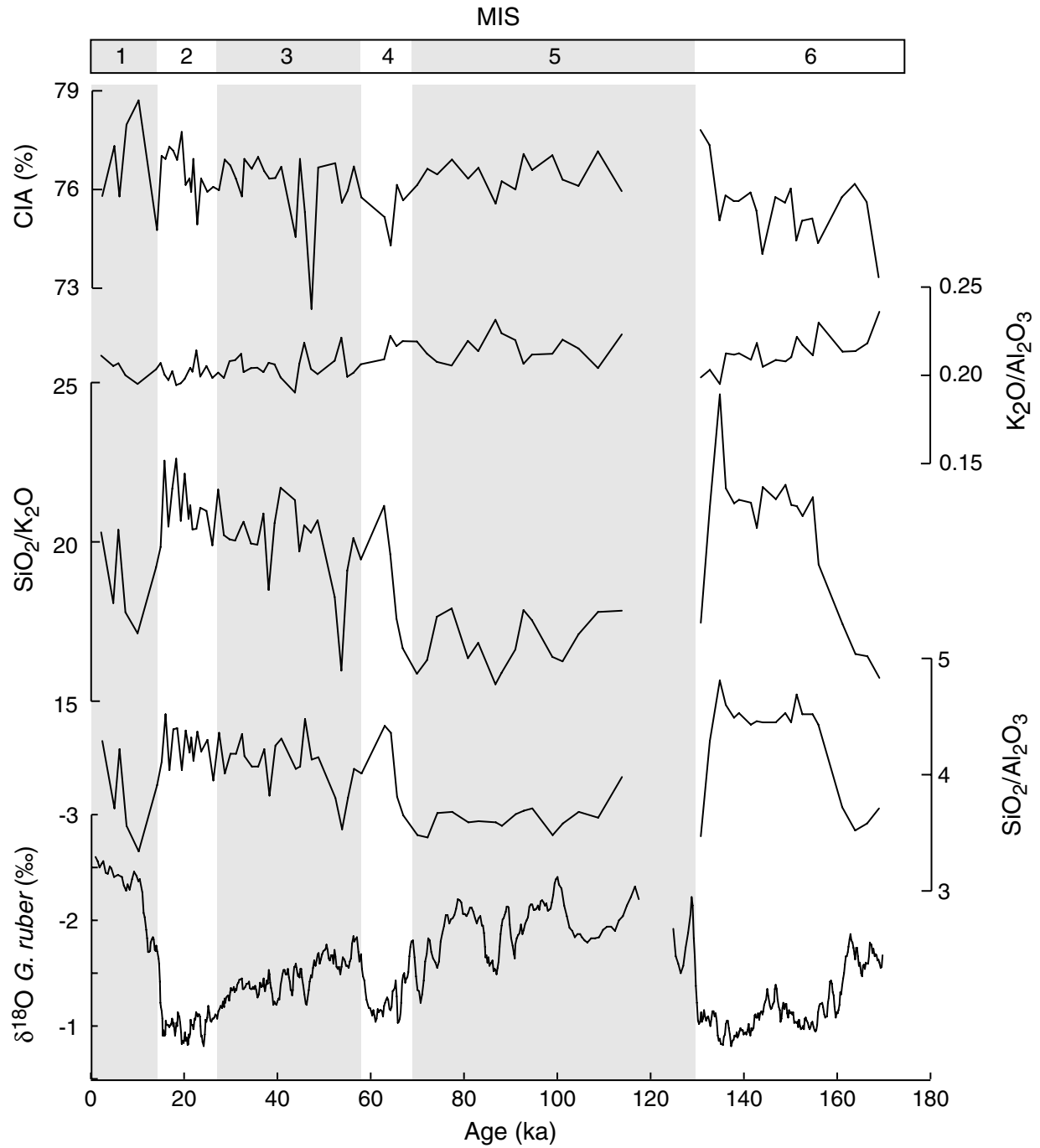**Figure F9.** Planktonic foraminifer *G. ruber* $\delta^{18}O$ record, reflectance (L*, lightness), $CaCO_3$, quartz, mean grain size, and SiO_2/Al_2O_3 ratio vs. age. MIS = marine isotopic stage.